PIER C

(Received 23 March 2026, Accepted 26 April 2026, Scheduled 8 May 2026)

Compact Designs of U-Slot Cut Hexagonal Microstrip Antennas Loaded with Shorting Posts for Circular Polarized Response

Amit A. Deshmukh*, Sujay Tawde, and Sanjay B. Deshmukh

Department of EXTC, SVKM's DJSCE, Mumbai, India

ABSTRACT: This paper presents the configurations of U-slot cut hexagonal microstrip antennas loaded with shorting posts, which realize a reduction in the center frequency of axial ratio bandwidth as well as the total substrate thickness. Three configurations employing four, eight, and twelve shorting posts positioned around a hexagonal patch are presented. Shorting posts loading adds to the inductive component in the antenna's input impedance, which yields a reduction in total substrate thickness and the frequency. Among three variations, U-slot cut hexagonal patch employing eight shorting posts yields the optimum result. It achieves axial ratio bandwidth of 2.23%, for $0.033\lambda_{cAR}$ reduction in the substrate thickness and 55 MHz (4.5%) reduction in the center frequency of axial ratio bandwidth. All these results are for a marginal reduction in peak broadside gain. Against the U-slot cut hexagonal patch on a reduced substrate thickness, shorting posts loaded antenna achieves higher axial ratio bandwidth with 56 MHz (4.81%) reduction in the center frequency of axial ratio bandwidth. Considering all these results, the proposed design offers a compact circular polarized solution, while employing a resonant U-slot. For the obtained antenna characteristics, the proposed designs can find applications in GPS L5 and L2 bands. Experimental validation for the proposed configurations has been carried out where the measured results show close agreement with simulated ones.

1. INTRODUCTION

Antennas that offer circularly polarized (CP) response are preferred at the receiver in wireless applications, as they minimize the signal loss arising from multi-path propagation effects [1]. To realize CP response, two equal amplitude signals satisfying the space and phase orthogonality are needed [1]. These conditions are easily achieved in a microstrip antenna (MSA), while suitable modifications are incorporated in the radiating patch or on the ground plane [2–4]. To obtain a CP response in MSA, various techniques have been reported in the literature. They are realized either by single patch excited using multiple feeds [5], or by embedding narrow slot in the patch and the placement of stubs on the patch edges [6, 7], or by selecting modified shape of the radiating geometry [8, 9], or by using multiple parasitic resonators in the planar or stacked layer of the fed patch [10–13], or by selecting resonant slot embedded inside the patch [14–19], or by embedding slot or fractal shape geometries on the ground plane [20–22]. Amongst these techniques, the selection of parasitic resonators or multiple resonant slots embedded inside the patch yields a wider axial ratio (AR) bandwidth (BW). To minimize the interference across different operating bands or to cater to multiple frequency bands of a specific wireless application using a single antenna, a multi-band CP MSA is required. Multi-band CP response is obtained by cutting a slot inside the patch, placing stubs on the patch edges, with the selection of multiple patches around the fed MSA, or using the reconfigurable antennas [23–28].

Amongst various techniques reported for CP response, resonant slot is an optimum choice, since it gives AR BW of 3–6%, peak gain of 7–9 dBic, while employing an air or air-suspended substrate. In air suspended variation, a lossy low-cost substrate can be used. In addition, suspended design makes the antenna results reliable against the variations in substrate parameters. A compact MSA is obtained, while positioning shorting posts on the patch [2, 3]. By placing multiple shorting posts at several positions on the rectangular patch, a CP response has been obtained in [29]. However, unlike the properties of the shorted patch, this shorted CP design does not offer a compact solution as it functions around the degenerated second-order resonant mode frequencies of the rectangular patch and thus has larger patch dimensions [30]. Therefore, while reported techniques are considered, methods to reduce the center frequency of AR BW (f_{cAR}) and the substrate thickness, to obtain a compact CP MSA, are not discussed.

In this paper, compact CP designs of U-slot cut hexagonal MSAs (HMSAs), which are loaded with shorting posts positioned around the patch periphery, are proposed for achieving a reduction in the center frequency of AR BW as well as the substrate thickness. Initially, in the 1200 MHz frequency range, the design of a U-slot cut HMSA for CP response is presented. On a total substrate thickness of 1.82 cm ($0.077\lambda_{cAR}$), the CP design yields AR BW of 52 MHz (4.26%) with a broadside peak gain close to 7 dBic. To achieve a compact CP solution while offering a reduction in the center frequency of AR BW and the substrate thickness, configurations of U-slot cut HMSAs loaded with either four, or eight, or twelve shorting posts are proposed. The shorting posts loading adds to the inductive reactance in the antenna's input impedance, which helps in optimizing U-slot HMSA on a reduced substrate thickness. For each of the configurations, a detailed parametric study for assessing the ef-

* Corresponding author: Amit A. Deshmukh (amitdeshmukh76@gmail.com).

fects of shorting posts loading on the center frequency of AR BW, substrate thickness, and antenna gain (efficiency), is carried out. Amongst the proposed configurations, the design employing eight shorting posts placed around the patch periphery yields an optimum result. On a substrate thickness of 1.02 cm ($0.044\lambda_{cAR}$), an eight-shorting-posts-loaded design yields an AR BW of 26 MHz (2.23%), with a peak broadside gain of above 6.5 dBic across the AR BW. Against the initial U-slot cut HMSA, shorting posts loaded MSA achieves $0.033\lambda_{cAR}$ reduction in the substrate thickness, while realizing 55 MHz (4.5%) reduction in the center frequency of AR BW. All these results are obtained for a marginal reduction in the peak broadside gain. To compare, the original CP configuration of U-slot cut HMSA is designed on a total substrate thickness 1.02 cm that yields an AR BW of 24 MHz (1.975%). In comparison, eight shorting posts loaded U-slot cut HMSA achieves a higher AR BW and provides 56 MHz (4.81%) reduction in the center frequency of the AR BW. All these frequency and substrate thickness reductions are obtained for a marginal decrement in the broadside antenna gain. Thus, considering the frequency and substrate thickness reduction together, the proposed design offers a compact CP solution while employing the resonant U-slot embedded inside the patch. In this process, a research gap for resonant U-slot cut MSAs in terms of higher substrate thickness and reduction in the center frequency of AR BW as well as higher patch size in shorted CP MSA is addressed. Considering these advances, the proposed design is novel in its research contribution. The proposed shorting posts loaded U-slot cut HMSAs are studied using Computer Simulation Technology (CST) simulation software [31], followed by the experimental validations. In the experimental validations, radio frequency (RF) instruments, namely, ZVH-8, FSC 6, and SMB 100A, have been used. The measurements have been carried out inside the Antenna laboratory, and they show a fairly close agreement with the simulations.

2. U-SLOT CUT HMSA LOADED WITH SHORTING POSTS FOR CP RESPONSE

The design of coaxially fed HMSA embedded with unequal length U-slot is shown in Figs. 1(a) and 1(b). In the proposed design, a three-layer suspended configuration is employed. It consists of two layers of low-cost FR4 substrate ($\varepsilon_r = 4.3$, $h = 0.16$ cm), separated by an air gap of thickness h_a cm. In this paper, a hexagonal patch and U-slot dimensions are optimized such that they address the frequencies around the GPS L5 and L2 bands. Therefore, initially for $h_a = 1.5$ cm, HMSA radius 'r' is optimized using the simulations such that TM_{11} mode frequency is around 1250 MHz. For this frequency and substrate parameters, HMSA radius is found to be 5.1 cm. On the hexagonal patch, the U-slot of dimension, $L_h \times L_v \times L_{h1} \times w_u$ (in cm) is cut as shown in Fig. 1(a). While employing the parametric optimization for the U-slot dimensions, an optimum CP response in the U-slot cut HMSA is achieved. The unequal lengths in U-slot degenerate the fundamental TM_{11} mode into diagonal orthogonal TM_{11}^{45} and TM_{11}^{135} resonant modes, and an optimum inter-spacing between them achieves a CP response [19]. The optimization process for the U-slot cut CP

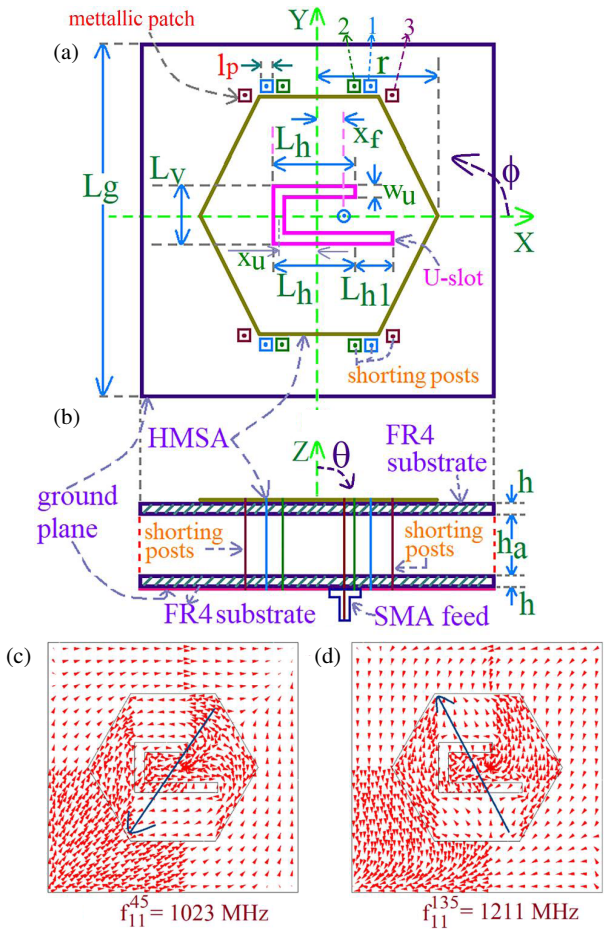

FIGURE 1. (a), (b) U-slot cut HMSA for CP response loaded with shorting posts, (antenna dimensions in cm), (c), (d) surface current distribution at degenerated modes in the CP design of the U-slot cut HMSA.

HMSA is similar to that present in U-slot cut cmSA, as explained in [19], and hence respective plots for the parametric optimization for U-slot cut CP HMSA are not shown. For the antenna dimensions as $h_a = 1.5$, $L_v = 3.0$, $L_h = 3.2$, $L_{h1} = 1.8$, $x_f = 0.6$ cm, the U-slot cut HMSA realizes a dual-band response. In the first band, HMSA offers a simulated reflection coefficient (S_{11}) BW of 128 MHz (10.74%), which includes a simulated AR BW of 52 MHz (4.26%). For the above U-slot and feed position, impedance matching is not achieved in the second band, as shown in Fig. 2(a); hence, the BW is not specified here. Across the first band, the antenna offers a broadside radiation pattern with a maximum gain of 7 dBic across the AR BW. In terms of the wavelength (λ_{cAR}) at the center frequency of AR BW, the substrate thickness in this CP design is $0.077\lambda_{cAR}$. The substrate thickness can be lowered, while ground plane modifications are employed [32]. However, these modifications increase the MSA radiation in the back lobe, which affects the broadside gain. Instead of ground plane modifications, shorting posts are employed in the antenna cavity. The shorting posts will add to the inductive reactance in the input impedance of the antenna. This increased inductive component in the antenna's input impedance can be reduced while lowering the total substrate thickness, i.e., by reducing the air gap in the three-layer suspended variation. In

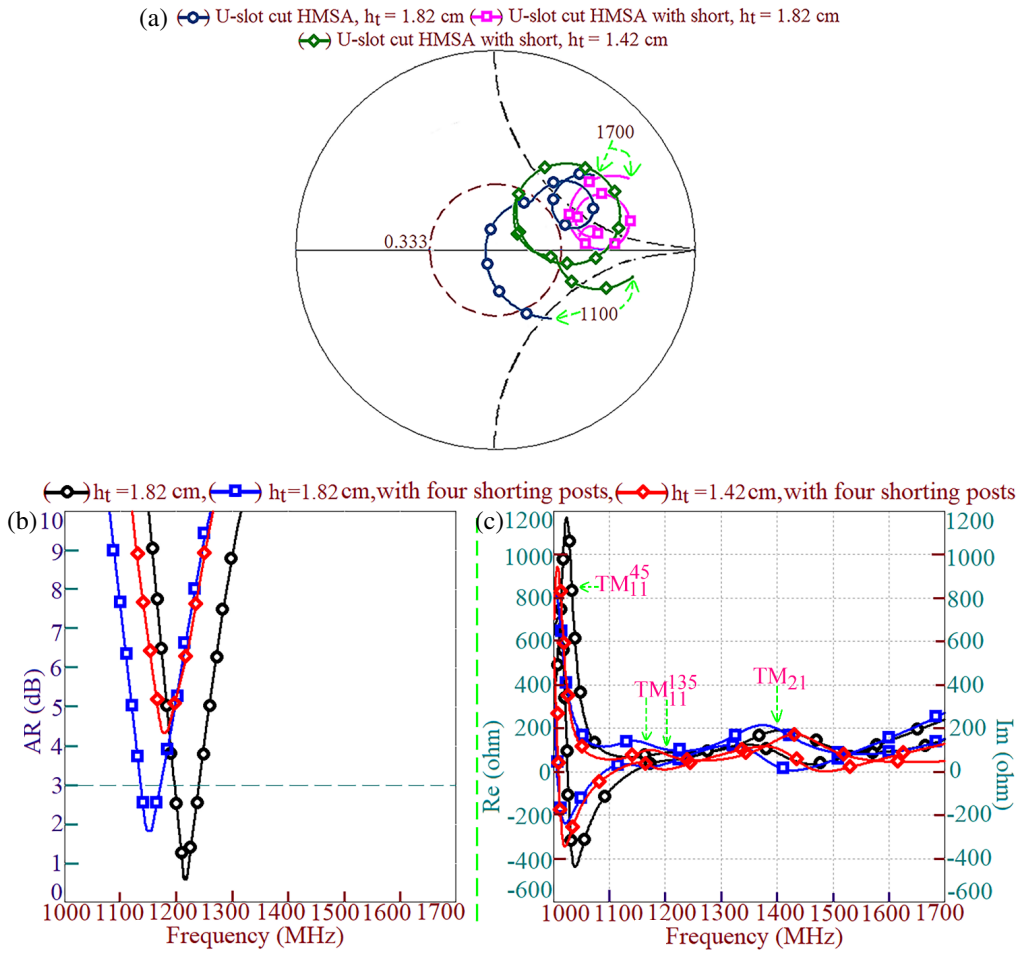

FIGURE 2. (a) Smith charts, (b) AR, and (c) resonance curve plots for U-slot cut HMSA and its shorting posts loaded variation against varying total substrate thickness.

this manner, the design will be realized on a reduced substrate thickness. The selection of the shorting posts position is an important design criterion, as they should minimally affect the antenna gain. If the shorting posts are positioned within the patch boundary, they will affect the resonant boundary conditions for the half wavelength U-slot cut hexagonal patch resonator and will affect its gain. Therefore, the shorting posts are positioned outside the patch boundary, near the diagonal points as shown in Figs. 1(a) and 1(b). This position is chosen since in the degenerated orthogonal modes in U-slot cut HMSA, currents vary along the two diagonal axes as shown in Figs. 1(c) and 1(d).

The shorting posts, each of 0.1 cm in diameter, are placed on a square metallic patch of length $l_p = 0.2$ cm. The shorting posts are placed in a close vicinity to the hexagonal patch, while maintaining a 0.1 cm air gap with respect to the patch edge. To assess the effects of shorting posts, initially, the study is carried out using four shorting posts positioned around the patch diagonal vertex points indicated by position '1', as shown in Fig. 1(a). In this study, the dimensions of the HMSA loaded with U-slot are kept the same. The Smith chart, resonance curve, and AR plots for this variation are provided in Figs. 2(a)–2(c). As mentioned above, the unequal length U-slot cut HMSAs on the total substrate thickness (h_t) of 1.82 cm achieves CP response around the frequency of 1220 MHz, as shown in Fig. 2(b).

Observing the resonance curve and AR plots, AR BW is obtained around TM_{11}^{135} mode frequency, due to its optimum spacing with respect to TM_{11}^{45} mode frequency. With the placement of four shorting posts, the inductive reactance in the input impedance of the antenna cavity increases, which makes the impedance locus positioned in the higher inductive region in the Smith chart, as observed from Fig. 2(a). This loading of shorting posts also increases the input impedance at TM_{11}^{135} mode. With this $S_{11} < -10$ dB BW is not obtained, which does not support the realization of CP response even for AR to be less than 3 dB, as observed from Fig. 2(b). It should be noted from Fig. 2(b) that the center frequency of AR BW (f_{cAR}) decreases with the shorting posts loading. In order to reduce the inductive reactance from the antenna input impedance, substrate thickness is reduced by lowering the air gap thickness h_a. The reduction in h_a (h_t) from 1.5 (1.82) to 1.1 (1.42) cm lowers the inductance due to the probe length, which optimizes the impedance locus inside VSWR = 2 circle in the Smith chart as mentioned in Fig. 2(a). The reduction in h_t affects the AR value, which is not optimized for less than 3 dB, to achieve a CP response, as observed from Fig. 2(b). With further optimization in U-slot dimensions here, optimum CP response is achieved, while four shorting posts are employed. Using this procedure, the optimum CP response for a lower value of h_t supported with

a reduction in f_{cAR} is obtained, by loading the shorting posts around the hexagonal patch periphery. Therefore, by using a simpler technique of shorting posts loading, antenna response is optimized on a reduced total substrate thickness. The optimization of the U-slot dimension on reduced substrate thickness so as to achieve optimum AR BW is a similar process, as present in the initial design of the U-slot cut HMSA. Hence, plots for those parametric optimizations are not provided here. Thus, by employing four shorting posts, an optimum AR BW is achieved for $h_a = 1.1$ cm. It is noted in the parametric study that with a further reduction in h_a below 1.1 cm, impedance locus does remain inside VSWR = 2 circle, but the input impedance at the orthogonal TM_{11}^{45} and TM_{11}^{135} modes decreases, which does not support AR < 3 dB for the CP response. Therefore, for the configuration employing four shorting posts, an optimum response is obtained for the antenna parameters as $r = 5.1$, $h = 0.16$, $h_a = 1.1$, $L_v = 3.0$, $L_h = 3.2$, $L_{h1} = 1.1$, $w_u = 0.6$, $x_f = 0.8$ cm, and results for the same are shown in Figs. 3 and 4.

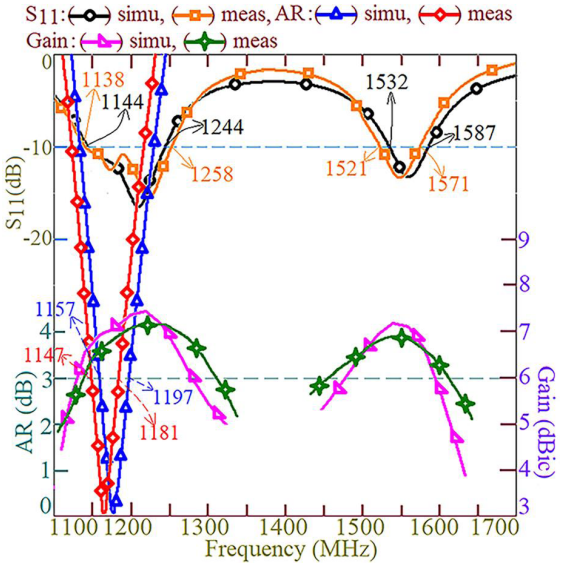

FIGURE 3. Optimum results for four shorting posts loaded U-slot cut HMSA.

Similar to the original U-slot cut HMSA on substrate thickness of 1.82 cm, the shorting posts loaded U-slot cut HMSA on the total substrate thickness of 1.42 cm offers dual-band response. In the simulation, the S_{11} BW observed in the two bands is 100 MHz (8.37%) and 55 MHz (3.52%), respectively. Against this in the measurement, respective S_{11} BWs observed in the dual bands are 120 MHz (10%) and 50 MHz (3.23%). The second band response in the U-slot cut HMSA is attributed to the second-order modified TM_{21} mode frequency [19]. In the first band, the U-slot cut HMSA offers a CP response. It gives simulated and measured AR BWs of 40 MHz (3.39%) and 34 MHz (2.92%), respectively. Over the two bands, the antenna offers a broadside radiation pattern with a peak gain of larger than 6 dBic over the AR and S_{11} BW. For a larger length in the bottom arm of the U-slot, the design offers a right-hand CP (RHCP) response in the first band. The presence of a U-slot on the hexagonal patch modifies the surface current distribution at TM_{21} mode and aligns the surface current components along the horizontal direction [19]. This yields broadside radiation at the modified TM_{21} mode and thus in the second band. Considering the simulated result, the center frequency of AR BW (f_{cAR}) is 1177 MHz, and the substrate thickness in terms of wavelength at the f_{cAR} is $0.059\lambda_{cAR}$ (1.42 cm). In comparison to the initial U-slot cut HMSA on the substrate thickness of 1.82 cm, four shorting posts loaded design offers a reduction in f_{cAR} by 42 MHz (3.44%). In addition, loading shorting posts offers $0.018\lambda_{cAR}$ reduction in the electrical substrate thickness. For further comparative assessment, the U-slot cut HMSA without loading the shorting posts is designed on the total substrate thickness of 1.42 cm. It gives a simulated AR BW of 41 MHz (3.34%). In comparison, shorting posts loaded design offers nearly the same AR BW but offers 48 MHz (4.07%) reduction in the f_{cAR}. Thus, loading four shorting posts achieves a reduction in the substrate thickness, as well as the frequency, thereby realizing a compact CP solution.

To achieve a further reduction in the substrate thickness and frequency, additional shorting posts are located at the position '2' as mentioned in Fig. 1(a). While positioning these additional four shorting posts, the spacing of 0.5 and 0.1 cm with respect to the initially located shorting posts and with respect to the patch edge, respectively, is maintained. The Smith chart, resonance curve, and AR plots, for the positioning of additional four shorting posts on the four shorting posts loaded U-slot cut HMSA for $h_t = 1.42$ cm, are shown in Figs. 5(a)–5(c). With additional shorting posts, i.e., in eight shorting posts loaded design, input impedance locus becomes inductive in nature. Although AR<3 dB is observed, across the frequencies around the center frequency of AR BW, impedance matching condition is not present, so as to obtain $S_{11} < -10$ dB BW.

The input impedance matching is realized by reducing the total substrate thickness, which lowers the probe inductance. This positions the impedance locus inside the VSWR = 2 circle to obtain $S_{11} < -10$ dB BW. Next, while optimizing the U-slot dimension, optimum CP response is obtained in eight shorting posts loaded design and antenna parameters in the same are $h_a = 0.7$, $h = 0.16$, $L_v = 3.0$, $L_h = 3.2$, $L_{h1} = 0.8$, $w_u = 0.6$, $x_f = 0.6$ cm. Results for this configuration are given in Fig. 6. Eight shorting posts loaded U-slot cut HMSA on the total substrate thickness of 1.02 cm offers a dual-band response. In the simulation, S_{11} BW observed in the two bands is 92 MHz (7.75%) and 69 MHz (4.15%), respectively. Against this in the measurement, respective S_{11} BW observed in the dual bands is 114 MHz (9.5%) and 67 MHz (4.05%). In the first band, U-slot cut HMSA offers CP response. It gives simulated and measured AR BWs of 26 MHz (2.33%) and 24 MHz (2.08%), respectively. Over the two bands, antenna offers a broadside radiation pattern with a peak gain of larger than 6 dBic over the AR and S_{11} BW. In the first band, the U-slot cut HMSA offers right-hand circular polarization (RHCP) radiation pattern. Considering the simulated result, the center frequency of AR BW (f_{cAR}) is 1164 MHz, and the substrate thickness in terms of wavelength at the f_{cAR} is $0.044\lambda_{cAR}$ (1.02 cm). In comparison to the initial U-slot cut HMSA on the substrate thickness of 1.82 cm, the eight shorting posts loaded design offers a reduction in f_{cAR} by 55 MHz (4.5%). In addition, shorting posts

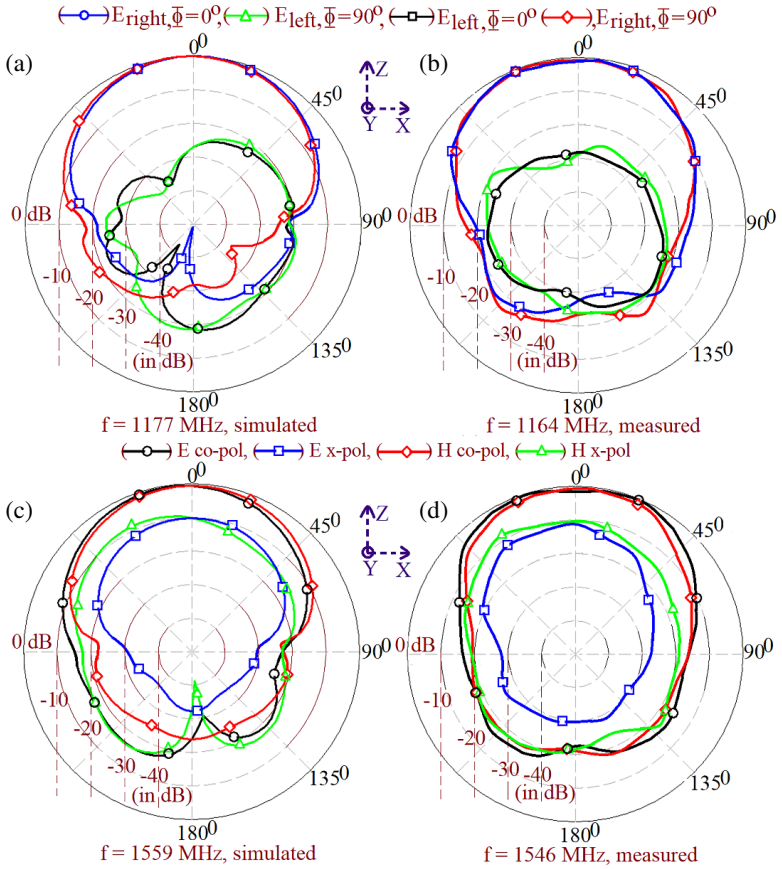

FIGURE 4. Radiation pattern at the center frequency of (a) (b) first and (c) (d) second band for four shorting posts loaded design of U-slot cut HMSA.

loading offers $0.033\lambda_{cAR}$ reduction in the electrical substrate thickness. The U-slot cut HMSA without the shorting posts loading is designed on the total substrate thickness of 1.02 cm. It gives simulated AR BW of 24 MHz (1.97%). In comparison, eight shorting posts loaded design offers higher AR BW with 56 MHz (4.81%) reduction in f_{cAR}. The CP response in the U-slot cut HMSA in the first band is attributed to the degeneration of the fundamental mode into dual orthogonal diagonally directed resonant modes. The modal degeneration is possible as modal surface currents exhibit half-wavelength variation along the patch resonant dimension [19]. At second-order TM_{21} mode, two-half-wavelength variation in modal currents is present that does not achieve mode degeneration with U-slot. Hence, the CP response is not present in the second band, to achieve a dual-band CP antenna.

Antenna measurement setup along with the fabricated prototype is shown in Fig. 7. The S_{11} BW measurement is carried out using ZVH-8 VNA. All the far-field measurements are carried out inside the Antenna laboratory. In this wideband, high-gain reference horn antennas are used. The pattern measurement is carried out using the automated pattern measurement setup, whereas broadside gain is measured using the three-antenna method. This method provides better accuracy, for the measurements inside the Antenna laboratory. The distance between the horn antenna and the antenna under test (AUT) is kept to be more than the minimum far-field distance, calculated with respect to the highest frequency of S_{11} BW in the respective band. However, for all the measurements in this paper, a far-field distance of 380 cm is chosen that satisfies the above condition in all the bands. In the laboratory setup, metallic objects are minimum in number around the central measurement desk. In addition, the distance of the surrounding wall from the central measuring desk is more than seven times the wavelength calculated with respect to the lowest frequency of S_{11} BW in the first band. All these details ensure minimum reflections from the surrounding objects in the far-field measurements and thus provide good agreement with the simulated results. For calculating the right-hand and left-hand CP components, the measurement of E-field in the two polarizations of the antenna is carried out, and then by using conversion equations, right- and left-hand field components are evaluated [33].

Circularly polarized radiation from the antenna is investigated by studying the time varying surface current distribution at the center frequency of AR BW and by using the far-field probes placed in the simulation. Respective surface currents, orthogonal E-fields, and phase plots are shown in Figs. 7(c)–7(f) and 8(a). With reference to the antenna, current vectors are rotated in clockwise direction. Near the CP frequency range, orthogonal radiated fields (E_x and E_y) are equal in magnitude. Here, the phase component φ_x is leading φ_y by 90^0. With reference to the antenna as a radiator and in the direction of propagation, surface currents, E-field magnitude, and its phase conditions, along with pattern plots shown above, confirm the clock-

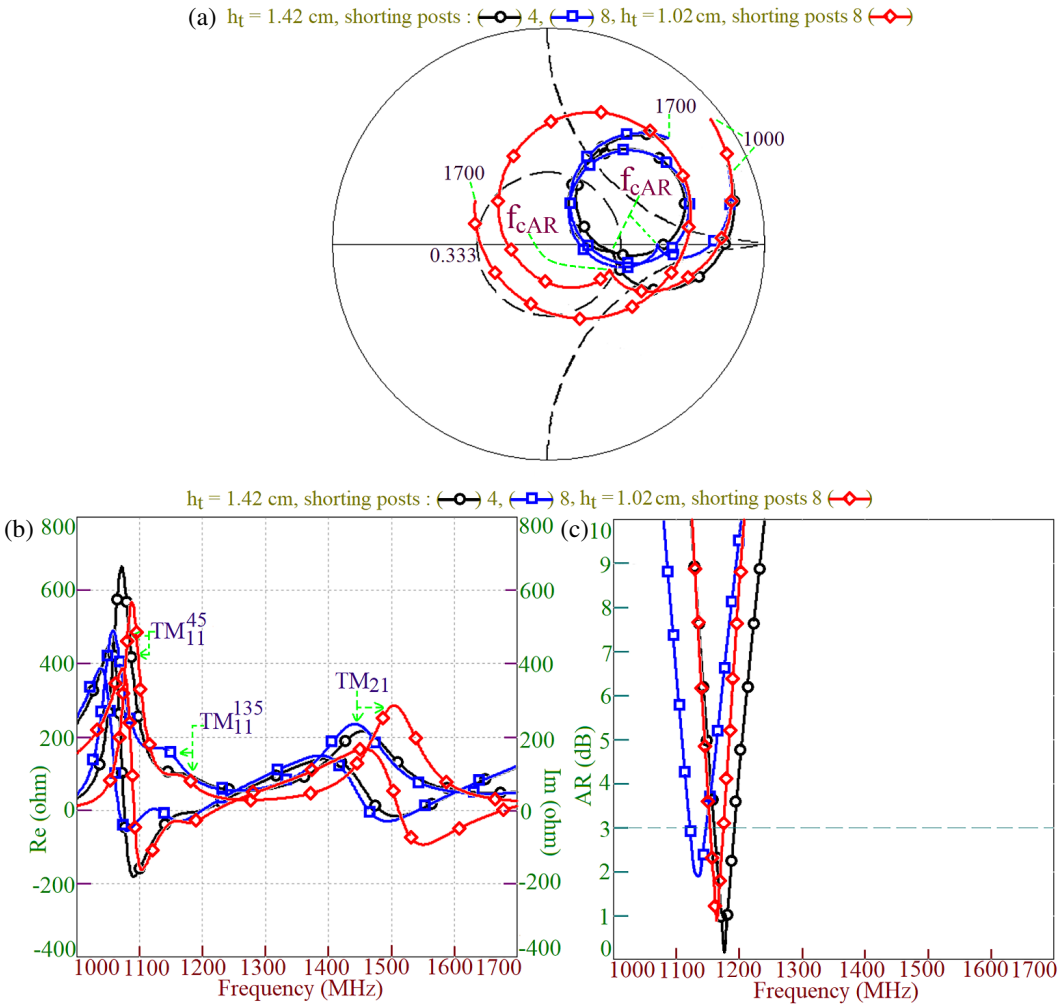

FIGURE 5. (a) Smith chart, (b) AR, and (c) resonance curve plots for U-slot cut HMSA loaded with four and eight shorting posts against varying total substrate thickness.

wise or RHCP radiated signal from the shorting posts loaded HMSA.

Further reduction in substrate thickness and the center frequency of AR BW is obtained while additional four shorting posts are placed at position '3', of the eight shorting posts loaded U-slot cut HMSA, as shown in Fig. 1(a). The position '3' is selected, since the same position is located around the patch diagonal vertex points of HMSA. This creates a cluster of shorting posts around the vertex points compared to being placed away from the patch diagonal points along the edge of the hexagonal patch. Similar to the four and eight shorting posts loaded U-slot cut HMSAs, parametric study is initiated from the eight shorting posts loaded HMSA. The corresponding Smith chart, resonance curve, and AR plots were studied to arrive at an optimum design using twelve shorting posts for offering maximum possible AR BW with a reduction in the total substrate thickness and f_{cAR}. This is obtained for $h_a = 0.5$ cm, and various antenna parameters in the optimum design are $h = 0.16$, $L_v = 3.0$, $L_h = 3.2$, $L_{h1} = 0.5$, $w_u = 0.6$, $x_f = 0.5$ cm. Results for twelve shorting posts loaded configuration are given in Figs. 8(b) and 9. Twelve shorting posts loaded U-slot cut HMSA on the total substrate thickness of 0.82 cm also offers a dual-band response. In the simulation, the S_{11} BW observed in the two bands is 69 MHz (5.91%) and 49 MHz (2.99%), respectively. Against this in the measurement, S_{11} BW observed in the dual bands is 71 MHz (6.11%) and 58 MHz (3.56%). In the first band, the U-slot cut HMSA offers CP response. It gives simulated and measured AR BWs of 20 MHz (1.74%) and 21 MHz (1.84%), respectively. Over the two bands, the antenna offers a broadside radiation pattern with a peak gain of larger than 5 dBic over the AR and S_{11} BW.

In the first band, the U-slot cut HMSA offers an RHCP radiation pattern. Considering the simulated result, the center frequency of AR BW (f_{cAR}) is 1147 MHz, and the substrate thickness in terms of wavelength at the f_{cAR} is $0.036\lambda_{cAR}$ (0.82 cm). In comparison to the initial U-slot cut HMSA on the substrate thickness of 1.82 cm, twelve shorting posts loaded design offers a reduction in f_{cAR} by 72 MHz (5.9%) and $0.041\lambda_{cAR}$ reduction in the electrical substrate thickness. The U-slot cut HMSA without loading the shorting posts is designed on a substrate with a total thickness of 0.82 cm. It gives a simulated AR BW of 18 MHz (1.5%). In comparison, twelve shorting posts loaded design offers a higher AR BW with 52 MHz (4.53%) reduction in the f_{cAR}. To analyze the effects of short-

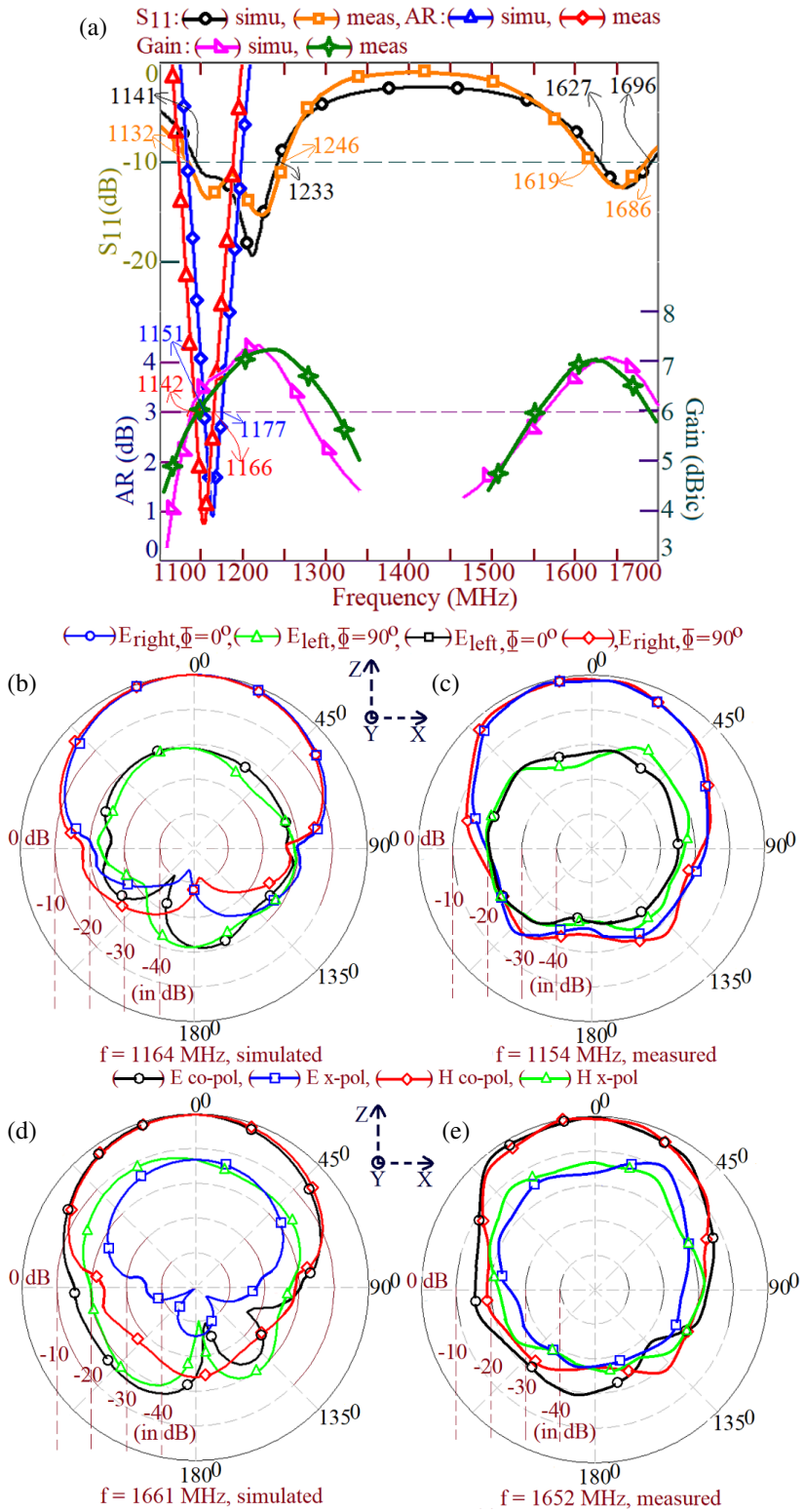

FIGURE 6. (a) S_{11}, AR BW and gain plots, and radiation pattern at the center frequency in the (b), (c) first and (d), (e) second band for U-slot cut HMSA loaded with eight shorting posts.

ing posts loading on the efficiency of the antenna, plots of antenna efficiency in four different configurations starting with the design of the U-slot cut HMSA are studied, and they are provided in Fig. 10(a).

As can be seen from the plots, against the design of U-slot cut HMSA without the loading of shorting posts, a marginal reduction in efficiency is noted in four and eight shorting posts loaded designs, whereas using a twelve shorting posts loaded design, the efficiency is decreased to around 60%, which re-

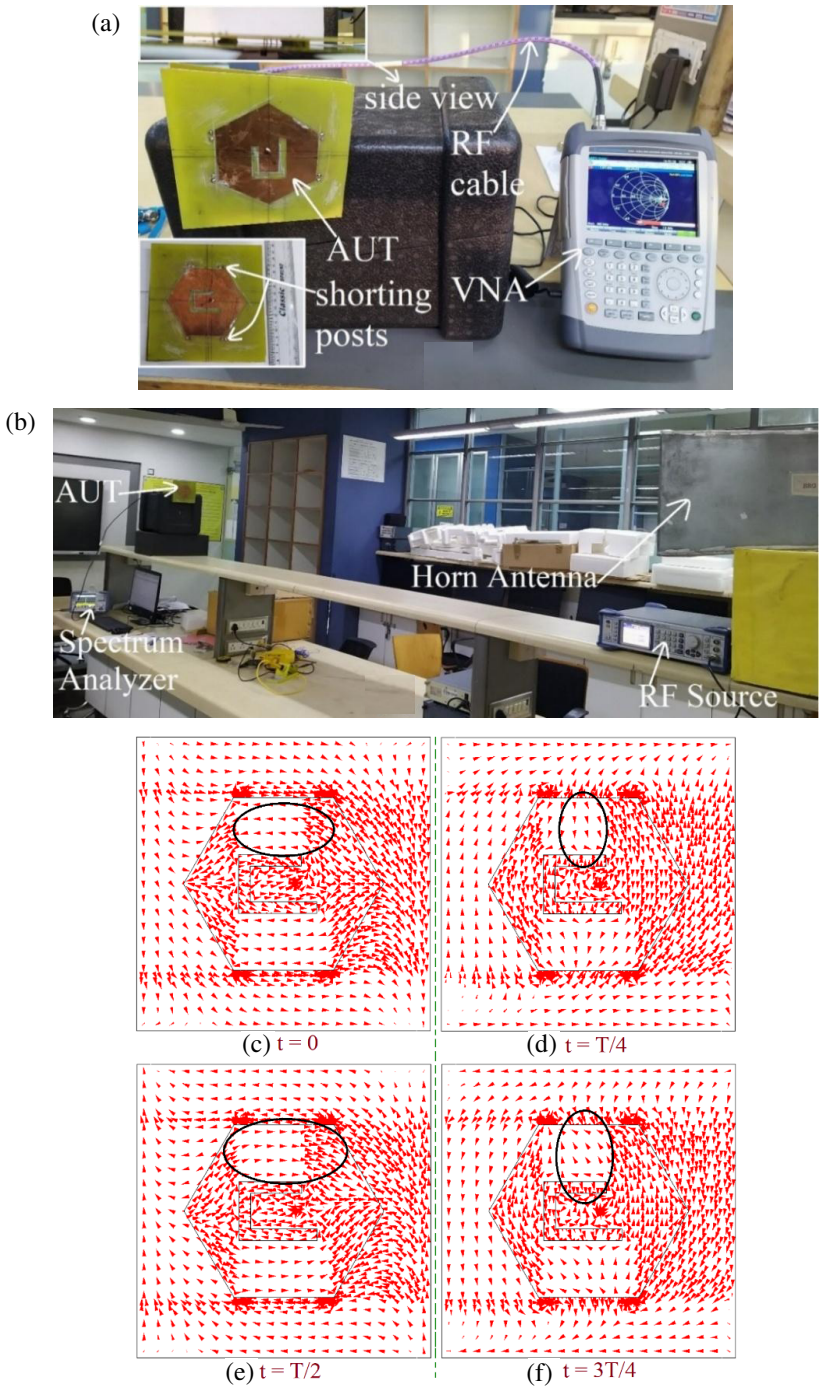

FIGURE 7. (a) S_{11} BW, (b) broadside gain, measurement setups, and (c)–(f) time varying surface current distribution at center frequency of AR BW for U-slot cut HMSA loaded with eight shorting posts.

duces the broadside gain as seen in Fig. 8(b). The efficiency appears to be improving in the second band. For understanding this improvement, broadside gain in the design of the U-slot cut HMSA without shorting posts loading, for $h_t = 1.82$ cm, is also analyzed. The peak gain here is around 6 dBi, which increases to nearly 7 dBi with the loading of shorting posts. To arrive at the explanation for this gain improvement, average and vector surface current distributions in the second band were studied without and with shorting posts loading, as shown in Figs. 10(b) and 10(c). It is noted that the surface current variation in magnitude and direction gets stronger along the horizontal direction over the antenna aperture. This effect dominantly leads to the gain improvement in the second band, while shorting posts are placed around the patch periphery. The design employing shorting posts positioned at (1) and (3), as shown in Fig. 1(a), is also studied. In this design, the reduction in the broadside gain below 6 dBic is noted across the AR BW. At the degenerated resonant modes, the maximum of the resonant fields exists near the HMSA vertex points. Due to the placement of shorting posts here, the antenna efficiency decreases to around 60% over

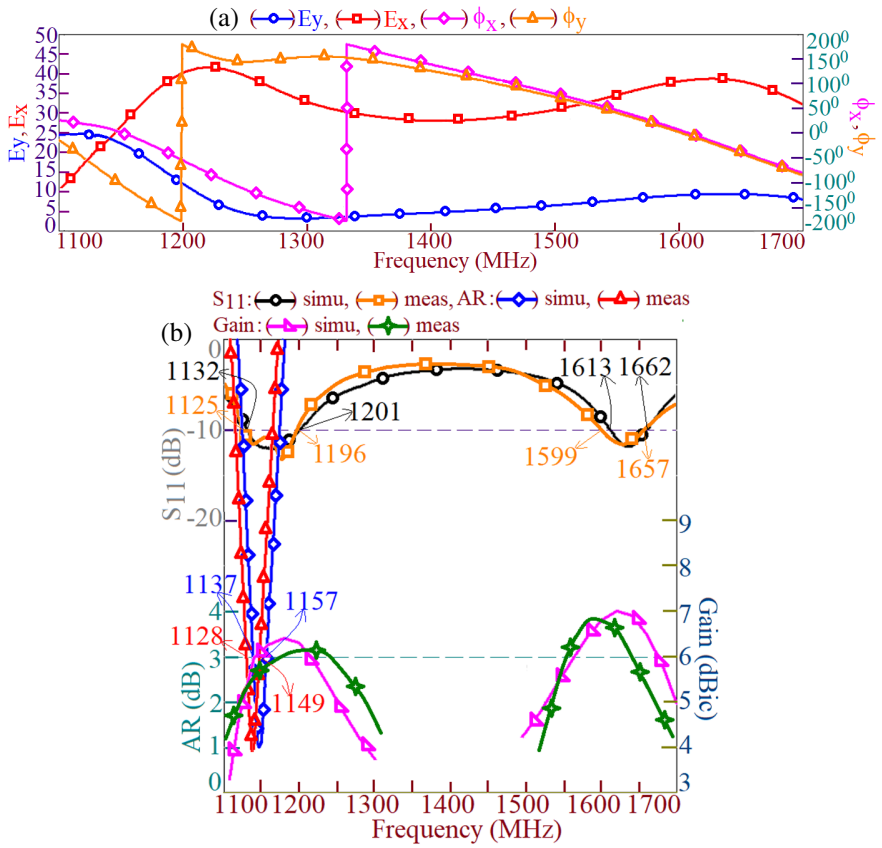

FIGURE 8. (a) Orthogonal E-field and phase plots for U-slot cut HMSA loaded with eight shorting posts, (b) S_{11}, AR BW and gain plots for U-slot cut HMSA loaded with twelve shorting posts.

the AR BW. In twelve shorting posts design also, the cluster of shorting posts is loaded near the patch vertex points. Due to the close proximity of shorting posts with patch vertex points, the efficiency and gain of the CP antenna decrease.

Hexagonal geometry has a similar resonant mode distribution to that of a circular patch. Thus, they offer suppression to the harmonic frequencies as supplied by the input RF source. However, compared to the circular edge in circular MSA, hexagonal geometry has a straight patch edge that enables the appropriate coupling/loading of shorting posts with the degenerated resonant modes of the U-slot cut patch. Thus, hexagonal geometry is selected in the present work.

3. DESIGN METHODOLOGY FOR SHORTING POSTS LOADED U-SLOT CUT HMSA

This section describes the design methodology for eight shorting posts loaded U-slot cut HMSA for CP response. Initially, resonant length formulations at various U-slot cut hexagonal patch modes are proposed. As seen from the resonance curve plots in the parametric study for the U-slot cut HMSA, loading shorting posts reduces the resonance frequencies of fundamental degenerated TM_{11} modes. In the equivalent circuit model, loading shorting posts adds an inductor in the equivalent circuit of the MSA, which reduces the resonance frequency. In the present approach, instead of a circuit model, the effects of shorting posts loading on the reduction in the resonance frequency are accounted for with an additional length, in addition to the length that contributes to the effects of U-slot on HMSA resonant modes. Beginning with the design of U-slot cut HMSA on the total substrate thickness of 1.02 cm, the resonant length formulation is proposed. For the antenna dimensions in the optimum design of eight shorting posts loaded HMSA, an effective hexagonal patch radius, without loading shorting posts and U-slot, is given by using Equation (1). The effective dielectric constant (ε_{re}) in the three-layer suspended design involving an FR4 substrate is calculated by using Equation (2), and the resonance frequency of TM_{11} mode is calculated by using Equation (3). For the antenna parameters mentioned above, calculated TM_{11} mode frequency is 1319 MHz, which agrees closely with the simulated frequency of 1320 MHz.

$$r_e = r + 0.73h_t \tag{1}$$

$$\varepsilon_{re} = \frac{\varepsilon_r^2\,(2h + h_a)}{2h\varepsilon_r + h_a\varepsilon_r^2} \tag{2}$$

$$f_{11} = 8.791/r_e\sqrt{\varepsilon_{re}} \tag{3}$$

The positioning of U-slot vertical length 'L_v' is not at the patch center, and hence, it offers a smaller reduction in HMSA's TM_{11} mode frequency. Therefore, effects of increment in equal lengths of horizontal U-slot length L_h along with length L_v are formulated together, and the effective patch radius accounting for both the lengths is given by using Equation (4). The resonance frequency of modified TM_{11} mode is calculated by using

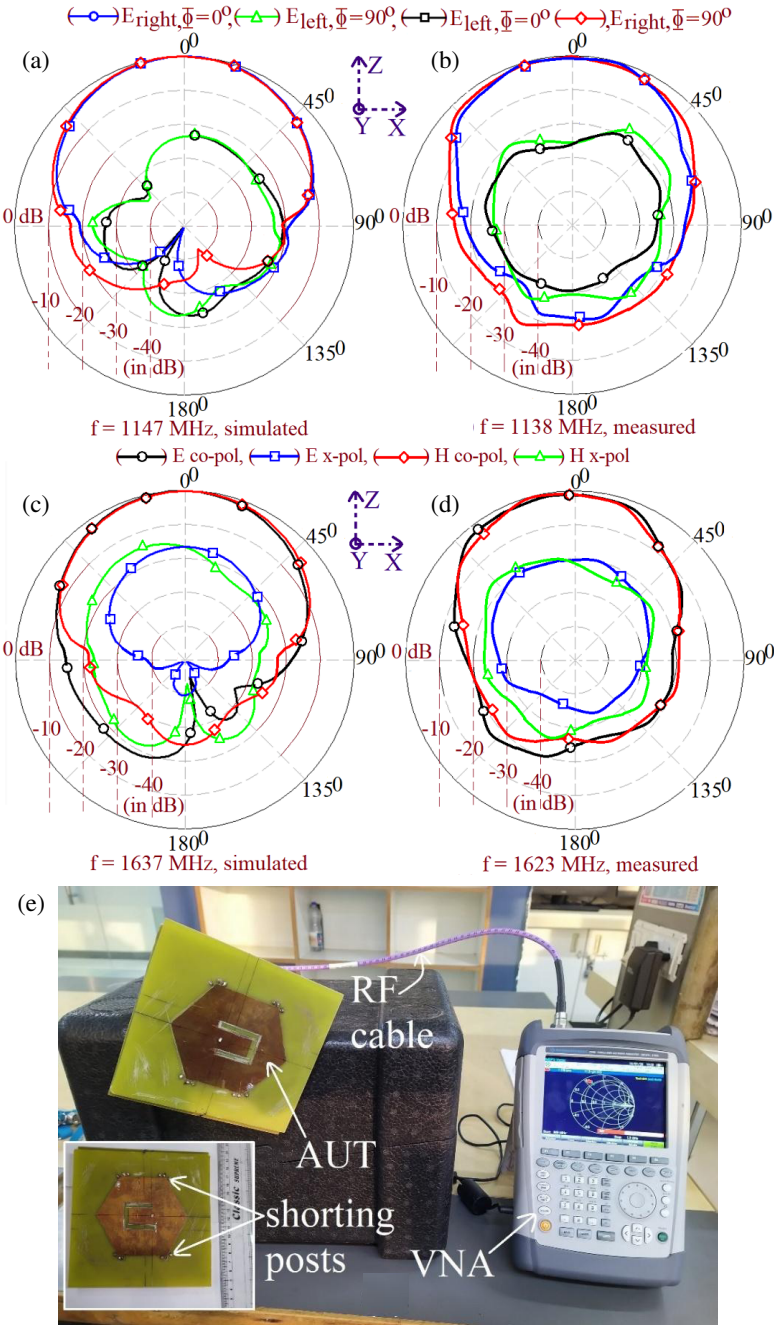

FIGURE 9. Radiation pattern at the center frequency of (a), (b) first and (c), (d) second band, and (e) S_{11} BW measurement setup showing the fabricated prototype for the U-slot cut HMSA loaded with twelve shorting posts.

Equation (3) for $r_e = r_{eh}$. For the above antenna parameters, the calculated TM_{11} mode frequency is found to be 1167 MHz compared to the simulated value of 1166 MHz.

$$r_{eh} = r + 0.73h_t + (L_v/25) + (L_h/5) \quad (4)$$

An unequal length 'L_{h1}' in the bottom arm of U-slot degenerates TM_{11} mode frequency into orthogonal and diagonal TM_{11}^{45} and TM_{11}^{135} mode frequencies. With an increment in L_{h1}, TM_{11}^{45} mode frequency decreases. An effective patch radius (r_{eh1}) that accounts for this frequency reduction is formulated by using Equation (5), and the frequency is calculated by using Equation (3) for $r_e = r_{eh1}$. The calculated frequency is found to be 1085 MHz against the simulated value of 1088 MHz.

$$r_{eh1} = r + 0.73h_t + (L_v/25) + (L_h/5) + (L_{h1}/1.6) \quad (5)$$

Using these formulations, the design methodology to realize eight shorting posts loaded U-slot cut HMSA is proposed. The CP response in the U-slot cut patch is attributed to the optimum inter-spacing between degenerated fundamental mode frequencies of the HMSA. Thus, a reduction in these frequencies with reference to the TM_{11} mode frequency of HMSA without a slot is also required to be maintained specifically, to realize an opti-

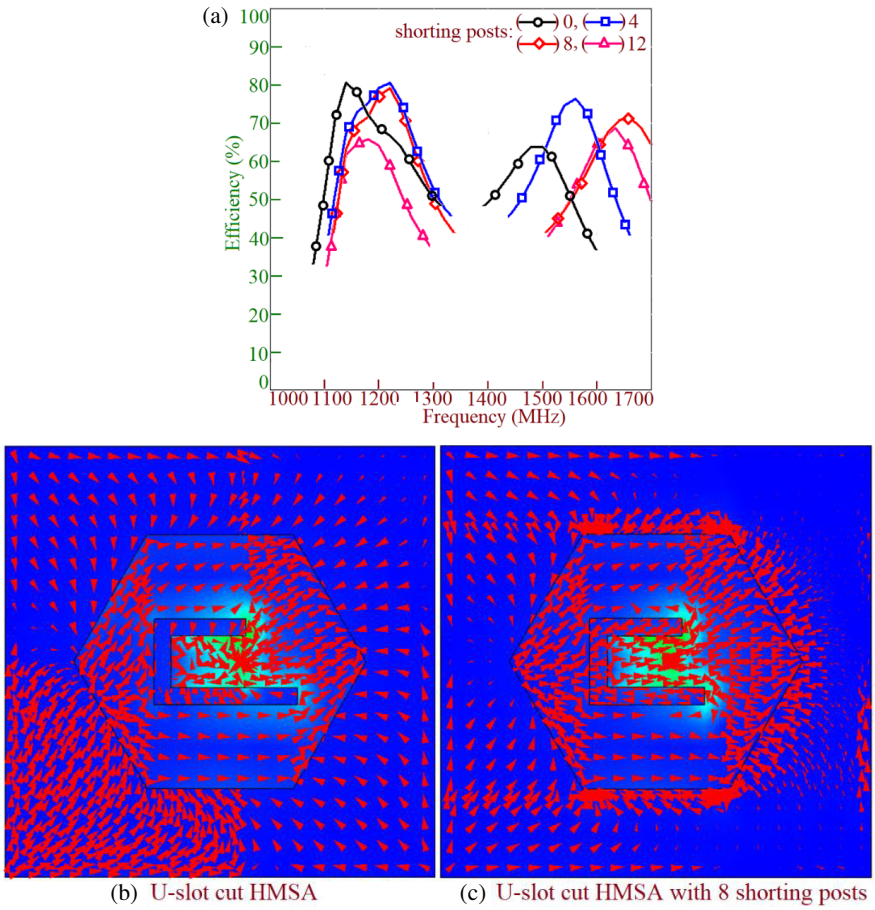

FIGURE 10. (a) Variation in the simulated antenna efficiency for U-slot cut HMSA against their shorting posts loaded variations, and (b), (c) surface current distribution in the second band without and with shorting posts loading.

mum CP response on a thinner substrate. Therefore, in addition to the above formulations, various frequency relations between modified resonant mode frequencies with reference to the center frequency of AR BW, present in the above optimum design, are selected in the design methodology. The methodology is initiated by specifying the center frequency of the desired AR BW, f_{cAR}. The total substrate thickness for the antenna is evaluated by using Equation (6). In this equation, the value of ε_{re} is not available to start with, since the air gap thickness is unknown. Therefore, the initial approximation of $\varepsilon_{re} = 1.25$ is considered. This approximation depends upon the value of ε_{re} as in the above optimum design for the mentioned substrate parameters. The calculated value of h_t equals $2h + h_a$, where h and h_a equal FR4 substrate and air gap thickness, respectively. Using this relation, h_a is obtained, which is an integer and practically realizable number. Next, using Equation (2), ε_{re} is recalculated for the obtained substrate parameters in a three-layer suspended design. This value is retained in all further calculations. The TM_{11} mode frequency of a hexagonal patch without U-slot and shorting posts loading bears a frequency relation, $f_{11} = 1.134 f_{cAR}$, with reference to the center frequency of AR BW. Using this fundamental mode, the frequency of the HMSA is obtained. For this frequency, the patch radius 'r' is calculated by using Equation (7).

$$h_t = 0.044\,(30/f_{\mathrm{cAR}}\sqrt{\varepsilon_{re}}) \quad (6)$$

$$r = (m8.791/f_{11}\sqrt{\varepsilon_{re}}) - 0.73h_t \quad (7)$$

The vertical U-slot length, along with equal arms of the horizontal U-slot lengths, reduces the TM_{11} mode frequency. This frequency bears a relation $f_{11Lh} = 1.003 f_{cAR}$ with reference to the center frequency of AR BW. Using this relation and Equation (8), effective patch radius r_{eLh} is calculated. Further, by using Equation (9), length L_h is obtained. While realizing Equation (9), the dimensional relation between U-slot lengths, as $L_v = 0.9375 L_h$, is used, and by simplifying and rearranging the terms on two sides of Equation (4), Equation (9) is obtained. The U-slot width is calculated as $w_u = 0.1875 L_h$.

$$r_{eLh} = 8.791/f_{11Lh}\sqrt{\varepsilon_{re}} \quad (8)$$

$$L_h = r_{eLh} - r - 0.73h_t/0.2375 \quad (9)$$

An unequal length in the bottom arm of U-slot degenerates TM_{11} mode frequency, and it further reduces TM_{11}^{45} mode frequency. This frequency bears a relation, $f_{11}^{45} = 0.9347 f_{cAR}$, with reference to the center frequency of AR BW. Using this relation and Equation (10), the effective patch radius r_{e11}^{45} is calculated. By using Equation (11), unequal U-slot length L_{h1} is evaluated. The position of vertical U-slot length from the patch center is selected as $x_u = 0.392r$, as mentioned in Fig. 1(a), whereas square ground plane length and coaxial feed position

TABLE 1. Results for the proposed U-slot cut CP HMSAs loaded with shorting posts.

U-slot cut HMSA loaded with	Meas. AR BW (MHz, %)	Peak Gain (dBic)	Substrate thickness h_t/λ_{cAR}
0 shorting posts	52, 4.26	7.0	0.077
4 shorting posts	34, 2.92	6.9	0.059
8 shorting posts	24, 2.08	6.6	0.044
12 shorting posts	21, 1.84	5.6	0.036

are calculated as $L_g = 2.941r$, $x_f = 0.1875L_h$.

$$r_{e11}^{45} = 8.791/f_{11}^{45}\sqrt{\varepsilon_{re}} \quad (10)$$

$$L_{h1} = 1.6\left(r_{e11}^{45} - r - 0.73h_t - (L_v/25) - (L_h/5)\right) \quad (11)$$

Using these formulations, eight shorting posts loaded U-slot cut HMSA is designed for $f_{cAR} = 915$ MHz. Various calculated antenna parameters are $h = 0.16$, $h_a = 1.0$, $r = 5.1$, $L_h = 4.2$, $L_{h1} = 1.0$, $L_v = 3.4$, $w_u = 0.8$, $x_u = 2.2$, $x_f = 1.0$, $L_g = 19.0$ cm. Eight shorting posts of 0.1 cm diameter are placed near the vertex points in the HMSA as shown in Fig. 1(a). The posts are placed on a square metallic patch of length $L_p = 0.2$ cm. The spacing between the hexagonal patch and shorting post center is maintained as 0.2 cm, whereas the spacing between two consecutive posts is maintained as 0.6 cm. The antenna is designed using these parameters, and the response is experimentally verified. In simulation, respective S_{11} BWs observed in the two bands are 74 MHz (7.9%) and 58 MHz (4.43%). Against this in the measurement, S_{11} BWs observed in the dual bands are 79 MHz (8.11%) and 62 MHz (4.71%), respectively. In the first band, the U-slot cut HMSA yields simulated and measured AR BWs of 21 MHz (2.29%) and 23 MHz (2.61%), respectively. Over the two bands, the antenna offers a broadside radiation pattern with a peak gain of larger than 6 dBic over the AR and S_{11} BW. The center frequency of AR BW in the first band is 916 MHz, which is very close to the initially selected frequency. This close agreement validates the proposed design methodology. Thus, employing the proposed design methodology, the eight shorting posts loaded HMSA embedded with a U-slot can be designed around a specific frequency, as per the given wireless application.

4. RESULTS DISCUSSION AND COMPARATIVE ANALYSIS

The U-slot cut MSA for CP response is an optimum design in terms of substrate used against the AR BW and gain realized. However, it requires a thicker substrate. Further, the employment of a U-slot does not highlight the reduction in the center frequency of AR BW, so as to achieve a compact CP solution. The study in this paper addresses both these research gaps and presents various configurations of shorting posts loaded U-slot cut HMSAs for the CP response. The designs presented achieve a reduction in the substrate thickness and a reduction in f_{cAR} compared to the U-slot cut HMSA without shorting posts. There have been many configurations presented in the literature on U-slot cut CP MSAs, but none of them achieves both these features together, and in terms of these details, the proposed configuration is novel in research contribution. A tabular comparison to highlight it is given in Table 2 and elaborated below. Amongst the proposed designs, the U-slot cut HMSA loaded with eight shorting posts achieves optimum results in terms of substrate thickness and f_{cAR} reduction against the AR BW and broadside gain, as mentioned in Table 1. Therefore, a comparison between the U-slot cut HMSA loaded with eight shorting posts and reported CP MSAs is tabulated in Table 2 and is discussed below. The reported configurations have been optimized in different frequency bands using different substrate thicknesses. Therefore, patch area and substrate thickness are normalized with respect to the wavelength at the center frequency of AR BW in each design. Considering the units, the area is normalized with respect to the square of the wavelength, whereas the substrate thickness is normalized with respect to the wavelength.

In the thinner substrate design discussed in [5], multiple feeding ports are employed with the help of a power divider circuit, which increases the design complexity of the antenna. The narrow slits cut design discussed in [6] offers a wide beamwidth CP response, but the AR BW is lower than 1%. Another thinner substrate design discussed in [7] employs a decoupled offset feed line, acting as a stub to excite the orthogonal modes on the patch. However, it also offers an AR BW lower than 1%. A partial ground plane modified ring-shaped printed antenna discussed in [8] offers a higher AR BW on a reduced substrate thickness. However, the antenna gain is smaller and requires larger patch dimensions than the proposed design. The overlapped square patch design (octagon shape) discussed in [9] on a thinner substrate has narrower AR BW. The multi-resonator CP MSAs discussed in [10–12] offer a higher AR BW than the proposed compact design. However, the addition of multiple resonators in different layers increases the antenna dimensions. Against this proposed configuration is a single-patch single-slot solution having a smaller size. The wideband CP MSA presented in [13] offers an AR BW of greater than 40%. However, it employs a multi-dielectric design employing multiple patches, shorting posts, and backed by a metallic cavity. All these design features increase the antenna substrate thickness as well as the design complexity. The CP MSAs employing a resonant U-slot discussed in [14, 15, 19] or multiple or modified slots cut CP MSAs discussed in [16, 17] offer the AR BW in the range of 4–20%. However, in none of these designs, techniques to lower the substrate thickness are discussed, nor are details provided for the reduction in the center frequency of AR BW. The wideband E-shape MSA discussed in [18] does offers a wider AR BW, but it requires a larger patch size attributed

TABLE 2. Comparison of the proposed U-slot cut CP HMSA against reported CP MSAs.

Refs.	Meas. AR BW (MHz, %)	Peak Gain (dBic)	Patch Area (A/λ_{cAR}^2)	Substrate thickness (h_t/λ_{cAR})
Fig. 1(a), eight shorting posts design	24, 2.08	6.7	0.125	0.044
[6]	23, 0.93	3.9	0.365	0.02
[7]	18, 0.72	10	0.06	0.023
[8]	46, 3.9	3.45	0.214	0.01
[9]	8, 0.5	3.9	0.442	0.02
[10]	250, 7.13	7.75	0.67	0.052
[11]	2090, 38.2	7.0	1.88	0.046
[12]	3040, 63.7	17.77	6.2	0.101
[13]	610, 42.8	4.8	0.685	0.189
[14]	90, 3.9	9.0	0.152	0.08
[16]	1000, 19	7.5	0.735	0.12
[17]	1160, 21.05	8.0	0.15	0.183
[19]	34, 3.78	8.3	0.137	0.069
[21]	6, 0.4	2.3	0.215	0.05
[22]	34, 1.38	5.2	0.139	0.054
[24]	1: 50, 1.02 2: 70, 1.26	1: 9.0 2: 8.6	2.82	0.047
[26]	9, 0.4 (band 1)	8.4	0.16	0.036
[27]	710, 28.4	10.1	> 1.65	0.105
[28]	79, 2.21 (band 1)	8.01	2.52	0.098
[31]	16, 0.653	7.6	0.51	0.04

to the assembly of multiple E-shape patches used. The modified ground plane design discussed in [20] has lower gain. The modified ground plane CP MSAs discussed in [21, 22] offer lower AR BWs and require thicker substrates and higher patch size than the proposed configuration. The reconfigurable multiple stubs loaded design discussed in [23] offers 33% frequency tuning range. However, over the same range, it suffers from the broadside gain variation by 6 dBic. With multiple patches fed by a long microstrip line, the dual-band design discussed in [24] requires a larger patch area. The dual-band half U-slot cut design discussed in [25] requires a larger substrate thickness. The proximity-fed multiple-patch dual-band CP MSA discussed in [26] offers lower AR BW in the first of its CP bands. The reconfigurable patch assembly of U-slot cut rectangular elements discussed in [27] offers a substantially higher AR BW but requires a much larger antenna size. The triple-frequency slot cut and stub-loaded microstrip line and aperture feed design discussed in [28] requires larger antenna dimensions. While placing multiple shorting posts on a rectangular patch, CP response has been realized in [29]. However, it offers a lower AR BW than the proposed shorting posts loaded design and requires a larger patch area. The larger patch area is attributed to the functioning of the configuration reported in [29] around degenerated second-order patch modes [3]. Against the design discussed in [29], the proposed design provides CP response around fundamental degenerated patch modes and thus possesses a smaller patch dimension. The U-slot cut MSA discussed in [34] only highlights the reduction in frequency compared to the conventional patch. Against this, the proposed design provides a reduction in substrate thickness in addition to the frequency. The tuning in the CP band frequency is realized using the reconfigurable approach as discussed in [35]. However, with the activation of PIN diodes, a frequency in the higher band is selected in [35]. In this regard, the MSA discussed in [35] does not provide any reduction in the AR BW center frequency, as provided in the proposed configurations.

To summarize, the proposed work presents designs of U-slot cut HMSAs for CP response, which are loaded with shorting posts around the patch periphery. In regard to configuration, the proposed work does not present a new design, but a simpler technique of shorting posts loading is selected, using which the reduction in the center frequency of the AR BW and the total substrate thickness is achieved, thus providing a resonant U-slot cut compact CP solution. Amongst all the configurations proposed, the MSA loaded with eight shorting posts offers optimum results. Eight shorting posts loaded HMSA offers a reduction in f_{cAR} by 55 MHz (4.5%) with a reduction in the electrical substrate thickness by $0.033\lambda_{cAR}$. Further, against the equivalent U-slot cut HMSA design with reduced substrate thickness, shorting posts loading offers a higher AR BW, with 56 MHz (4.81%) reduction in the f_{cAR}. In the literature, similar configurations of resonant U-slot or rectangular slots cut MSAs, which provide a reduction in both these parameters together, are not discussed, and in terms of these findings, the proposed

work is novel in its contribution. The loading of shorting posts shows minimal effect on the broadside gain. The configurations with the further loading of shorting posts, i.e., beyond twelve, were also studied. However, they show a reduction in the antenna efficiency and broadside gain. Hence, the present study is restricted to a twelve-shorting-posts-loaded design.

A small variation in the measured results compared to the simulation is observed. It is attributed to the errors in the measurement, specifically the air gap present in thinner substrate designs and a few fabrication tolerances. With a reduction in substrate thickness, the obtained AR BW is lower than 5%. Considering the BW, limitations do exist as the proposed design cannot cover multiple adjoining frequency bands of a given wireless application. However, for obtained antenna characteristics, the proposed compact designs can find applications in addressing specific individual GPS bands, such as L5 and L2. While maintaining a single-patch single-slot thinner substrate design, AR BW can be increased by selecting modifications in the ground plane. However, it will reduce the broadside gain. Thus, there will exist a trade-off between the BW improvement and the reduction in broadside gain.

5. CONCLUSIONS

The resonant slot cut CP MSA is an optimum design solution, considering the air-suspended configuration used against the obtained AR BW and broadside gain. However, in those designs, a reduction in the center frequency of AR BW supported with a substrate thickness reduction is not observed. The present study addresses this research gap and proposes the configurations of U-slot cut HMSAs loaded with multiple sets of shorting posts. The loading of shorting posts adds to the inductive reactance in the input impedance of the antenna that helps in lowering substrate thickness as well as the frequency. Amongst all the designs, the configuration realized using eight shorting posts yields optimum results. It offers a reduction in the center frequency of AR BW by 55 MHz (4.5%), supported with substrate thickness reduction by $0.033\lambda_{cAR}$. Against the equivalent reduced substrate thickness U-slot cut HMSA design, shorting posts loading offers 56 MHz (4.81%) reduction in the center frequency of AR BW. With all these reductions, broadside gain remains above 6 dBic. With the obtained antenna characteristics, the equivalent of the proposed designs can find applications in the GPS L5 and L2 frequency bands.

REFERENCES

[1] Balanis, C. A., *Antenna Theory: Analysis and Design*, John Wiley & Sons, 1996.

[2] Kumar, G. and K. P. Ray, *Broadband Microstrip Antennas*, Artech House, 2003.

[3] Garg, R., *Microstrip Antenna Design Handbook*, Artech House, 2001.

[4] Guha, D. and Y. M. M. Antar, *Microstrip and Printed Antennas: New Trends, Techniques and Applications*, John Wiley & Sons, 2011.

[5] Almalki, M., B. Alshammari, and S. K. Podilchak, "Dual-circularly polarized single-element patch antenna with compact multiport feeding," *IEEE Antennas and Wireless Propagation Letters*, Vol. 23, No. 2, 648–652, 2024.

[6] Ray, M. K., K. Mandal, and N. Nasimuddin, "Low-profile circularly polarized patch antenna with wide 3 dB beamwidth," *IEEE Antennas and Wireless Propagation Letters*, Vol. 18, No. 12, 2473–2477, 2019.

[7] Zhao, Z., F. Liu, J. Ren, Y. Liu, and Y. Yin, "Dual-sense circularly polarized antenna with a dual-coupled line," *IEEE Antennas and Wireless Propagation Letters*, Vol. 19, No. 8, 1415–1419, 2020.

[8] Agrawal, N., A. K. Gautam, and R. Mishra, "Design of low volume circularly polarized annular ring-shaped planar antenna for GPS applications," *International Journal of RF and Microwave Computer-Aided Engineering*, Vol. 31, No. 7, e22698, 2021.

[9] Shi, Y. and J. Liu, "A circularly polarized octagon-star-shaped microstrip patch antenna with conical radiation pattern," *IEEE Transactions on Antennas and Propagation*, Vol. 66, No. 4, 2073–2078, 2018.

[10] Wu, Q.-S., X.-Y. Tang, X. Zhang, L. Zhu, G. Zhang, and C.-B. Guo, "Circularly-polarized patch antennas with enhanced bandwidth based on capacitively coupled orthogonal patch radiators," *IEEE Open Journal of Antennas and Propagation*, Vol. 4, 472–483, Apr. 2023.

[11] Wang, Z., H. Luo, J. Dong, M. Wang, J. Tong, C. Xiao, J. Zheng, and R. Wu, "Wearable broadband circularly polarized antenna with characteristic mode analysis for wireless body area network applications," *IEEE Antennas and Wireless Propagation Letters*, Vol. 24, No. 6, 1312–1316, 2025.

[12] Verma, A., M. Arrawatia, and G. Kumar, "High gain wideband circularly polarized microstrip antenna array," *IEEE Transactions on Antennas and Propagation*, Vol. 70, No. 11, 11 183–11 187, 2022.

[13] Li, M., J. Yu, X. Shen, L. N. Lemma, D. Zeng, and Z. Yi, "Compact broadband GNSS antenna with wide AR beamwidth," *IEEE Antennas and Wireless Propagation Letters*, Vol. 24, No. 10, 3301–3305, 2025.

[14] Lee, K. F., K. M. Luk, W. C. Mok, and P. Nayeri, "Single probe-fed circularly polarized patch antennas with U-slots," *Microwave and Optical Technology Letters*, Vol. 53, No. 6, 1245–1253, 2011.

[15] Chen, Y. and C.-F. Wang, "Characteristic-mode-based improvement of circularly polarized U-slot and E-shaped patch antennas," *IEEE Antennas and Wireless Propagation Letters*, Vol. 11, 1474–1477, 2012.

[16] Mondal, T., S. Maity, R. Ghatak, and S. R. B. Chaudhuri, "Design and analysis of a wideband circularly polarised perturbed psi-shaped antenna," *IET Microwaves, Antennas & Propagation*, Vol. 12, No. 9, 1582–1586, 2018.

[17] Zeng, J., X. Liang, L. He, F. Guan, F. H. Lin, and J. Zi, "Single-fed triple-mode wideband circularly polarized microstrip antennas using characteristic mode analysis," *IEEE Transactions on Antennas and Propagation*, Vol. 70, No. 2, 846–855, Feb. 2022.

[18] Rahmat-Samii, Y. and J. M. Kovitz, "Wideband E-shaped patch antennas for advanced wireless terminals," *Advanced Electromagnetics*, Vol. 12, No. 2, 1–19, 2023.

[19] Deshmukh, A. A. and T. P. Page, "Unequal length U-slot cut design of polygon shape microstrip antenna for dual band response," *International Journal of Microwave & Optical Technology*, Vol. 18, No. 2, 153, 2023.

[20] Kumar, Y., R. K. Gangwar, and B. K. Kanaujia, "Compact broadband circularly polarized Hook-shaped microstrip antenna with DGS plane," *International Journal of RF and Microwave Computer-Aided Engineering*, Vol. 28, No. 6, e21275, 2018.

[21] Wei, K., J. Y. Li, L. Wang, R. Xu, and Z. J. Xing, "A new technique to design circularly polarized microstrip antenna by fractal

defected ground structure," *IEEE Transactions on Antennas and Propagation*, Vol. 65, No. 7, 3721–3725, 2017.

[22] Khajevandi, A. and H. Oraizi, "Design of a circularly polarized microstrip slot antenna using minkowski fractal by the characteristic mode theory," *Electronics Letters*, Vol. 58, No. 9, 352–355, 2022.

[23] Nguyen-Trong, N., L. Hall, and C. Fumeaux, "A frequency- and polarization-reconfigurable stub-loaded microstrip patch antenna," *IEEE Transactions on Antennas and Propagation*, Vol. 63, No. 11, 5235–5240, 2015.

[24] Ta, S. X., K. K. Nguyen, C. Dao-Ngoc, N. Nguyen-Trong, and e. al., "Single-layer, dual-band, circularly polarized, proximity-fed meshed patch antenna," *IEEE Access*, Vol. 10, 94 560–94 567, 2022.

[25] Deshmukh, A. A., A. Viswanathan, P. Nadkarni, V. A. P. Chavali, and H. Mistry, "Reconfigurable designs of equilateral triangular microstrip antennas for single and dual band circular polarized response in GSM and GPS applications," *AEU — International Journal of Electronics and Communications*, Vol. 193, 155729, Mar. 2025.

[26] Liang, Z.-X., D.-C. Yang, X.-C. Wei, and E.-P. Li, "Dual-band dual circularly polarized microstrip antenna with two eccentric rings and an arc-shaped conducting strip," *IEEE Antennas and Wireless Propagation Letters*, Vol. 15, 834–837, 2016.

[27] Dong, H., Y. Xiao, S. Tan, J. Hu, and Z. Chen, "Dual-broadband circularly polarized reconfigurable antenna based on asymmetric U-slot patch," *IEEE Antennas and Wireless Propagation Letters*, Vol. 22, No. 12, 3052–3056, 2023.

[28] Chen, W.-W., Q.-S. Wu, and X. Zhang, "Unified design of dual-band and triband dual-sense circularly polarized patch antennas under quad-mode operation," *IEEE Antennas and Wireless Propagation Letters*, Vol. 24, No. 6, 1332–1336, 2025.

[29] Zhang, X., L. Zhu, and N.-W. Liu, "Pin-loaded circularly-polarized patch antennas with wide 3-dB axial ratio beamwidth," *IEEE Transactions on Antennas and Propagation*, Vol. 65, No. 2, 521–528, 2017.

[30] Deshmukh, A. A., A. P. C. Venkata, A. G. Ambekar, and T. Sawant, "Analysis of multiple shorting posts loaded square microstrip antenna for circular polarized response," in *Proceedings of International Conference on Wireless Communication*, 207–214, Springer, Singapore, 2022.

[31] CST Software, Version 2019.

[32] Chavali, V. A. P. and A. A. Deshmukh, "Wideband designs of regular shape microstrip antennas using modified ground plane," *Progress In Electromagnetics Research C*, Vol. 117, 203–219, 2021.

[33] Toh, B. Y., R. Cahill, and V. F. Fusco, "Understanding and measuring circular polarization," *IEEE Transactions on Education*, Vol. 46, No. 3, 313–318, Aug. 2003.

[34] Deshmukh, A. A., J. Manek, and A. G. Ambekar, "Circularly polarized variations of truncated corner square microstrip antennas employing a U-slot," *IETE Journal of Research*, Vol. 71, No. 2, 554–565, 2025.

[35] Deshmukh, A. A. and V. A. P. Chavali, "Reconfigurable designs of U-slot cut microstrip antennas for dual band circularly polarized response," *Progress In Electromagnetics Research B*, Vol. 116, 1–18, 2026.